COBEM 2023 27TH INTERNATIONAL CONGRESS OF MECHANICAL ENGINEERING

ABCM Brazilian Society of Mechanical Sciences and Engineering
27th ABCM International Congress of Mechanical Engineering
December 04-08, 2023, Florianópolis-SC, Brazil

COB-2023-1245
NUMERICAL STUDY OF AIRFOIL IN NEAR-STALL CONDITIONS

Renan Trevizan de Melo
Daniel Sampaio Souza
Elmer Mateus Gennaro
Universidade Estadual Paulista "Júlio de Mesquita Filho" (Unesp) – Campus of São João da Boa Vista, São João da Boa Vista, SP 13876-750, Brazil
renan.trevizan@unesp.br
daniel.s.souza@unesp.br
elmer.gennaro@unesp.br

Abstract. *This research analyzes different flows over an airfoil in order to demonstrate a practical methodology to visualize the formation of laminar separation bubbles (LSB) with interest in characterize its main aspects. It is known that LSB appear as aerodynamic performance limiters in many flows, especially at low Reynolds numbers, and may affect the controllability of air vehicles in near stall conditions. Phenomena such as boundary layer separation, laminar-turbulent transition and vortex shedding are strongly linked to LSB. In this context, the Eppler 387 airfoil was characterized using the XFLR5 software and evaluated via CFD through the OpenFOAM to obtain LSB in a configuration close to the stall, with an angle of attack of 8º for steady state and Reynolds of 4.5×10^4 and 6×10^4. The distributions of pressure (and friction) considering laminar and turbulent flow were compared, identifying the formation of a short LSB ($Re = 6\times10^4$), with a separation at 0.148c and reattachment at 0.464c, and another long bubble ($Re = 4.5\times10^4$), with separation at 0.173c and reattachment at 0.682c (in terms of the airfoil chord, c). Evaluating the behavior of this type of instability can be decisive to understand its transition (bursting phenomena) and optimize prediction and control methods.*

Keywords: *laminar separation bubbles, aerodynamic performance, stall, prediction, control.*

1. INTRODUCTION

The aerodynamics of airfoils is strongly linked to the laminar flow that runs through them, and the separation of this flow is typically associated with harmful effects. A separate flow of interest is the laminar separation bubble, formed near the leading edge of thin airfoils by increasing the angle of attack (Melvill Jones, 1934).

Laminar separation bubbles often arise due to adverse pressure gradient and can be a limiting factor of aerodynamic performance, especially at low Reynolds number (Gaster, 1963; Mitra and Ramesh, 2019). The formation and disappearance of the separation bubbles produce non-stationary forces, making it challenging to design a new section of the airfoil.

In conditions close to stall, the substantial variations observed in the properties of the separation bubbles can also generate asymmetries in the aerodynamic forces of semi-wings, generating significant moments that will affect the controllability of the (Burgmann and Schroder, 2008) airplane, especially of micro air vehicles.

Therefore, the study of laminar separation bubbles represents a significant challenge since they involve a large number of phenomena, such as boundary layer separation (Balzer and Fasel, 2016), laminar-turbulent transition (Diwan *et al.*, 2006), vortex shedding (Pier, 2002), among others, as shown in Fig. 1. Additionally, other phenomena may arise due to bubble instability, such as flapping (Passaggia *et al.*, 2012), bursting (Gaster, 1963; Diwan *et al.*, 2006; Mitra and Ramesh, 2019) and the bypass transition (Zhao and Sandberg, 2020). Flapping is the oscillation of the bubble size, bursting is the sudden change in its characteristics (long-short or short-long), and the bypass transition corresponds to the one that does not go through the known mechanisms of primary and secondary instability of the boundary layer (Rodríguez *et al.*, 2021).

Bubble bursting results in a significant loss of lift, which can lead to an airfoil stall. Given its relevance, empirical and semi-empirical criteria for bursting prediction are widely used in current engineering correlations, and increasingly refined models have tried to characterize this phenomenon (Gaster, 1963; Diwan *et al.*, 2006; Mitra and Ramesh, 2019).

The location and size of the bubble directly depend on the airfoil shape, the angle of attack, and the Reynolds number. In addition, it can be seen that the angle of attack and the Reynolds number greatly influence the degree of free flow turbulence, and from this, in the size, structure, and characteristics of the laminar separation bubble (Burgmann and Schroder, 2008).

In this context, it is relevant to know the conditions under which a relatively short laminar separation bubble suddenly changes into a longer bubble. As observed in the literature, this condition affects the typical pressure distribution (Mitra and Ramesh, 2019), increases the drag, and, therefore, precedes the airfoil stall, resulting in a significant loss of lift. Therefore, it is interesting to characterize the separation bubble because of criteria such as the separation and reattachment points, bubble height, and reverse flow level.

Furthermore, traditional methods used in airfoil analysis are not always sufficient to predict bursting, and understanding

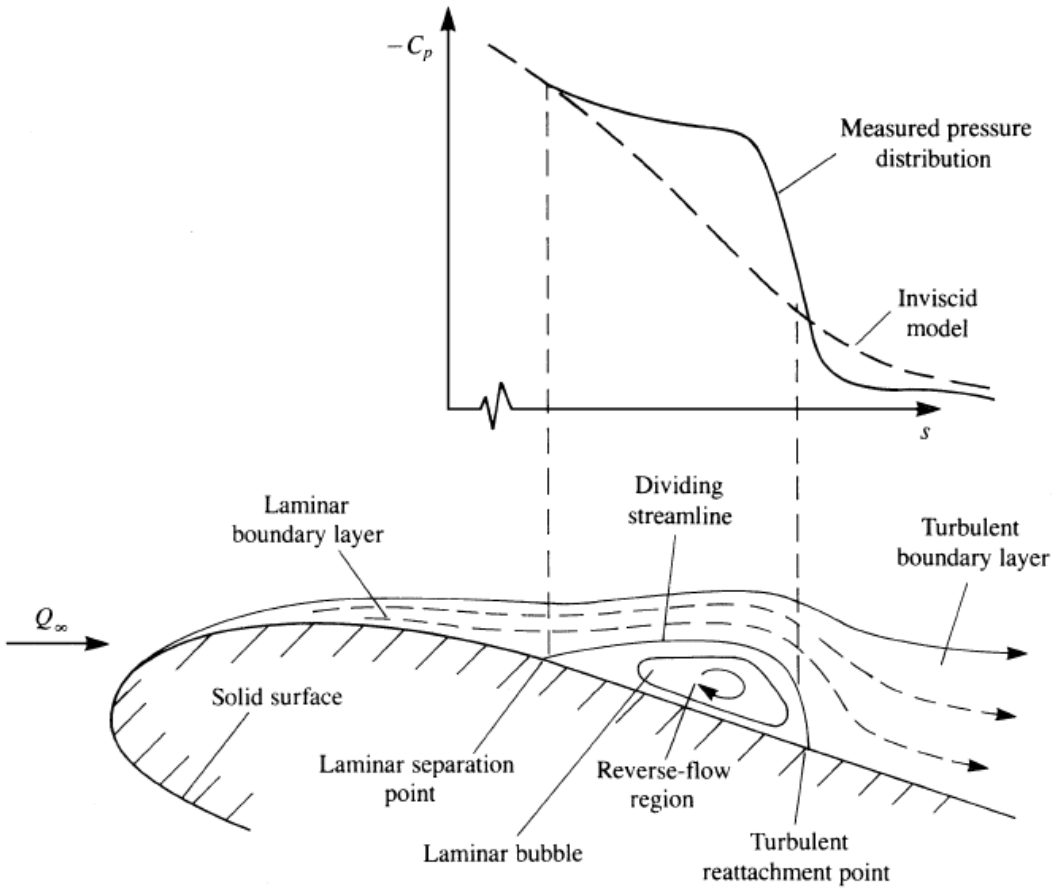

Figure 1. Schematic description of the transition from laminar to turbulent boundary layer and laminar bubble in an airfoil showing by Katz and Plotkin (2001).

the emergence of flow instabilities in bubble separation can contribute to improving these methods (Avanci *et al.*, 2019).

Thus, this work aims to provide ideas to conceive, theoretically, methodologies for analysis and prediction of the effects of flow on the airfoil and may contribute to the improvement of prediction methods for the transition point. This contribution is also directly related to the possibility of reducing drag and, consequently, reducing operating costs. It is noteworthy that the prediction of the transition point has the potential to delimit better stall control techniques, reducing the risk of aircraft crashes under these conditions.

2. CFD ANALYSIS

Computational Fluid Dynamics (CFD) uses numerical methods and computational algorithms to simulate the behavior of fluids in motion, a technique widely used in several branches of engineering. In CFD analysis, mathematical algorithms translate the physical equations responsible for describing the phenomena associated with flow, such as the Navier-Stokes equations (Ferziger and Peric, 2012).

2.1 Mathematical equations

The governing equations of CFD problems are so important for modeling and simulating the various phenomena described. Ferziger and Peric (2012) presents, as fundamental equations, the mass, momentum and energy conservation equations. Combining these equations for the three Cartesian dimensions results in the Navier-Stokes equations (Çengel and Cimbala, 2013).

According to Versteeg and Malalasekera (2007), the mass conservation equation, also known as the continuity equation, describes the temporal variation of the fluid density and can be written as Eq. (1):

$$\frac{\partial \rho}{\partial t} + \nabla \cdot (\rho \boldsymbol{v}) = 0 \tag{1}$$

Where ρ is the density of the fluid, t is the time, $\boldsymbol{v}$ is the velocity vector and $\nabla\cdot$ represents the divergent operator.

The linear momentum conservation equation is the second fundamental equation, which describes the temporal variation of the fluid's momentum and can be written, according to Moukalled *et al.* (2015), as Eq. (2):

$$\frac{\partial}{\partial t}(\rho \boldsymbol{v}) + \nabla \cdot (\rho \boldsymbol{v}\boldsymbol{v}) = -\nabla p + \mu \nabla^2 \boldsymbol{v} + \rho \boldsymbol{g} \tag{2}$$

Where p is the pressure, μ is the dynamic viscosity, ∇^2 represents the Laplacian operator and $\boldsymbol{g}$ is the gravitational vector. Each term describes one of the forces acting on the fluid and how they combine to produce its motion.

The third fundamental equation is the energy conservation equation, which, according to Ferziger and Peric (2012), describes the temporal variation of the fluid's energy, so that each term represents a source or destination of energy, and can be written as Eq. (3):

$$\frac{\partial}{\partial t}(\rho e) + \nabla \cdot (\rho e \boldsymbol{v}) = \nabla \cdot (k \nabla T) + \nabla \cdot (\boldsymbol{q}) + \rho \dot{q} \tag{3}$$

Where e is the specific energy, T is the temperature, k is the thermal conductivity, $\boldsymbol{q}$ is the heat flux vector, and $\dot{q}$ is the heat generation rate.

The set of expressions presented constitute the Navier-Stokes equations in their most general conservative form, being extremely complex. By assuming the fluids treated as Newtonian, defined as those for which the shear stress is linearly proportional to the strain rate, and considering the flow incompressible and approximately isothermal, that is, with small or non-existent local changes in temperature, the dynamic viscosities and kinematics become constants (Çengel and Cimbala, 2013), enabling numerical solution and analysis.

In short, for the presented conditions, we started to deal only with the continuity and momentum equations to describe the behavior of the fluid, simplifying the Navier-Stokes equations. In Cartesian form, for incompressible flow, 3D, at steady state as Eq. (4, 5, 6 and 7) (Moukalled *et al.*, 2015):

$$\frac{\partial u}{\partial x} + \frac{\partial v}{\partial y} + \frac{\partial w}{\partial z} = 0 \tag{4}$$

$$u\frac{\partial u}{\partial x} + v\frac{\partial u}{\partial y} + w\frac{\partial u}{\partial z} = -\frac{\partial p}{\partial x} + \nu\left(\frac{\partial^2 u}{\partial x^2} + \frac{\partial^2 u}{\partial y^2} + \frac{\partial^2 u}{\partial z^2}\right) \tag{5}$$

$$u\frac{\partial v}{\partial x} + v\frac{\partial v}{\partial y} + w\frac{\partial v}{\partial z} = -\frac{\partial p}{\partial y} + \nu\left(\frac{\partial^2 v}{\partial x^2} + \frac{\partial^2 v}{\partial y^2} + \frac{\partial^2 v}{\partial z^2}\right) \tag{6}$$

$$u\frac{\partial w}{\partial x} + v\frac{\partial w}{\partial y} + w\frac{\partial w}{\partial z} = -\frac{\partial p}{\partial z} + \nu\left(\frac{\partial^2 w}{\partial x^2} + \frac{\partial^2 w}{\partial y^2} + \frac{\partial^2 w}{\partial z^2}\right) \tag{7}$$

Where u, v and w are the velocity components in cartesian directions and ν represents the kinematic viscosity. In addition to the characterization of the flow given by the Navier-Stokes equations, turbulence models can be used in order to approximate the simulation of the desired turbulence levels in relation to a given reference case for the correct characterization of the underlying phenomena (Moukalled *et al.*, 2015).

RANS-type simulations are based on the time average of the Navier-Stokes equations, and consider that the flow properties vary only within a time average value. Therefore, it assumes the existence of a temporal average of the flow magnitudes and uses turbulence models to close the system of equations. These models include equations for turbulent viscosity and calculate the average effect of turbulence on flow (Ferziger and Peric, 2012).

Among the turbulence models most used in RANS-type simulations ($k-\omega\ SST$, $K-\varepsilon$, Spalart-Allmaras), the Spalart-Allmaras is recognized for its robustness in aerodynamic applications, as discussed by Spalart and Allmaras (1992) in his strategies for turbulence modeling and simulations. Its conception is based on a transport equation for a variable called turbulent viscosity, which can be understood by a composition of terms of diffusion, production and destruction in the wall (airfoil surface), being represented in the form:

$$\frac{\partial \tilde{\nu}}{\partial t} + \nabla \cdot (\tilde{\nu}\mathbf{U}) = c_{b1}\tilde{S}\tilde{\nu} - c_{w1}f_w\left(\frac{\tilde{\nu}}{d}\right)^2 + \nabla \cdot \left[\left(\nu + \frac{\tilde{\nu}}{\sigma}\right)\nabla\tilde{\nu}\right] + c_{b2}\nabla\tilde{\nu} \cdot \nabla\tilde{\nu} \tag{8}$$

where, $\tilde{\nu}$ is the turbulent kinematic viscosity; t demarcates the time; $\mathbf{U}$ corresponds to the average velocity vector; c_{b1} and c_{b2} are modeling constants; $\tilde{S}$ comprises the filtered strain rate tensor; f_w is a wall bound function; d characterizes the turbulent dissipation length; ν represents molecular kinematic viscosity; and σ encompasses a turbulent diffusivity constant.

2.2 Numerical modeling

For the construction of a solution algorithm and numerical analysis, the discretization of the problem is an essential part regarding CFD tools. Discretization consists of the process of dividing a continuous domain into a discrete mesh of points, cells or elements, where the governing equations are solved (Ferziger and Peric, 2012).

The finite volume method (FVM) comprises, according to Ferziger and Peric (2012), a numerical technique widely applied in this context, being used to solve partial differential equations in continuous domains. The method consists of discretizing the domain into small finite volumes, called cells or control volumes, in which the governing equations are solved.

The FVM is based on the conservation of physical quantities, such as mass, momentum and energy, within control volumes. For each cell, the conservation equations are integrated over its volume and expressed in the form of algebraic equations. The objective is to determine the values of the solution in each control volume, from the known values in the neighboring cells and in the boundary conditions (Versteeg and Malalasekera, 2007). One of the main advantages of FVM is that it allows dealing with complex geometries and inhomogeneous flows. Furthermore, it allows the analysis of problems in which the fluid and boundary properties vary in time and space.

It should be noted that the choice of mesh type and its refinement have a great influence on the accuracy and efficiency of the solution, according to Ferziger and Peric (2012). In this sense, the application of structured meshes provides high precision in relation to the exact solution, since they are characterized by elements or control volumes identical in shape and size, allowing greater control over the discretization of the domain and the accuracy of the solution (Ferziger and Peric, 2012).

Among the structured meshes, the C-type meshes comprise topologies frequently used in aerodynamics problems due to their ability to produce accurate and stable results. Type C meshes receive this name because of their similarity to this capital letter in a plan view. They comprise topologies in which the aerodynamic body is surrounded by lines that can also be adapted to form the wake region Hirsch (2007). This is a mesh frequently used in aerodynamic problems due to its ability to produce precise and stable results. The advantages of type C meshes include their ease of construction, low computational cost and the ability to minimize interpolation errors in regions of high gradients Blazek (2015).

An essential part of the analysis is also centered on the correct choice of boundary conditions, since they describe the physical conditions at the boundary of the calculation domain and allow the definition of how the fluid should interact with the walls and interfaces. Incorrect boundary conditions can, for example, lead to spurious flows, numerical instabilities and even divergence of the iterative process (Blazek, 2015).

Dirichlet boundary conditions specify the value of the variable of interest (for example, velocity or pressure) at the domain boundary. Neumann boundary conditions specify the value of the gradient of the variable of interest on the boundary of the domain Ferziger and Peric (2012). For external flow problems, such as flow around bodies, the boundary conditions are usually Dirichlet type at the body surface and Neumann type at the (Ferziger and Peric, 2012) boundaries.

In general, the sequential solution of the governing equations is widely used, allowing the iterative solution of the problem for a considered flow (Patankar, 1980). OpenFoam comprises one of the most used computational tools in this type of analysis, and has pre-implemented algorithms capable of solving the equations of varied flows.

Among the algorithms available in OpenFoam, SIMPLE (*Semi-Implicit Method for Pressure-Linked Equations*) is widely used in CFD simulations due to its simplicity and effectiveness in solving the Navier-Stokes equations for incompressible flows Patankar and Spalding (1972). The iterative process involves calculating the velocity and pressure field and correcting the pressure to satisfy Poisson's equation for pressure.

The accuracy of numerical solutions depends on the number of iterations that are performed and, therefore, it is important to have adequate convergence criteria to guarantee that such solutions are sufficiently accurate. In the residuals criterion, which is based on comparing the residuals of the iterative solution with a specified threshold value, when the residual value reaches the threshold, the solution is considered convergent and the iterative process is stopped Ferziger and Peric (2012).

3. SIMULATION METHOD

For this work, we chose the Eppler 387 airfoil (Figure 2) in order to analyze the characteristics and behavior of the flow around it under conditions close to stall. The selection of this airfoil was made due to its wide applicability, extensive documentation and asymmetric geometry (Eppler, 2013).

This is an airfoil often used in light aircraft designs, such as gliders and ultralights, due to its ability to provide good lift at low speeds and moderate angles of attack. The aerodynamic efficiency of the Eppler 387 airfoil also makes it a common choice for wind turbine blades (Eppler, 2013). Therefore, this is a geometry with well-documented features established in the scientific literature, which facilitates its use and analysis in different contexts (Eppler, 2013; Mitra and Ramesh, 2019).

The mesh used in the analyzes was built using *software* Gmsh (Geuzaine and Remacle, 2009), being structured type C, with refinement in the boundary layer and wake regions (Figure 3). For its creation, it is necessary to define the object of study, in addition to a computational domain in its surroundings, the region in which the flow will be defined. This region

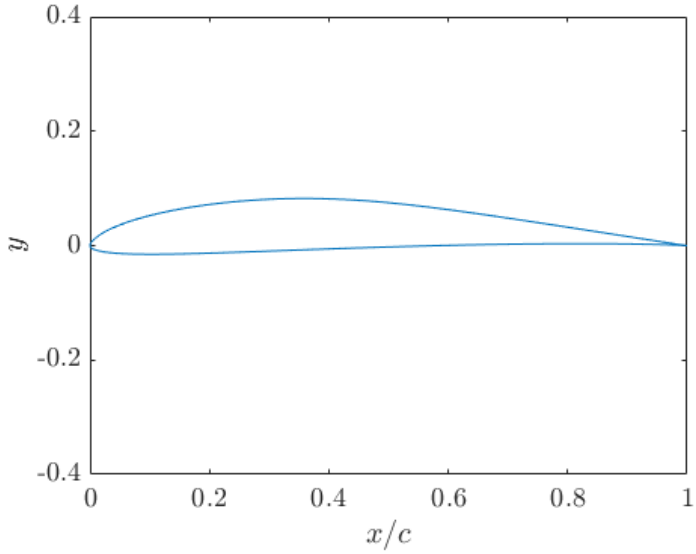

Figure 2. Eppler 387 Airfoil Geometry.

is divided into three main parts: input, upstream; on the wall, around the airfoil; and outgoing, downstream.

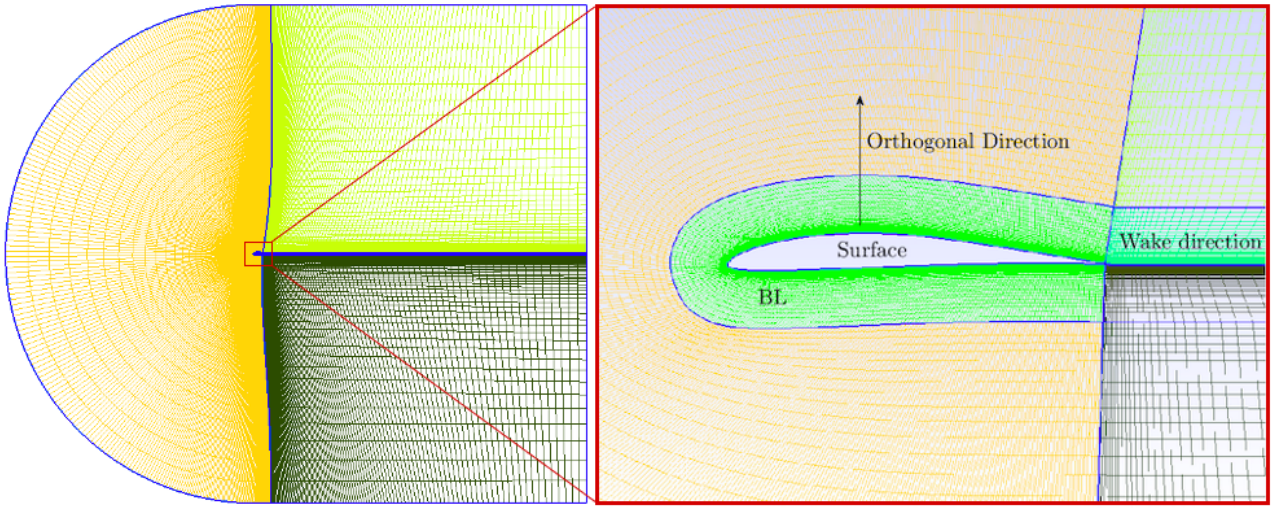

Figure 3. (a) General resolution view of the Type C mesh applied to the case study. (b) Enlarged view of the mesh.

In the mesh, identified in general view in Figure 3(a) and enlarged view in Figure 3(b), the inlet (in orange, extending in the direction orthogonal to the surface), the boundary layer (in green, around the airfoil) and the wake (in darker shades of green, downstream of the airfoil) stand out.

In order to evaluate the influence of the global mesh refinement level on the response obtained for the elaborated modeling, a convergence analysis was conducted. This study makes it possible to identify the discretization level from which there is no longer a significant oscillation of the output parameters.

Table 1 lists the mesh parameters investigated in this study. In particular, it is noteworthy that the parameter y^+ was kept close to 1. The y^+ corresponds to a parameter used in numerical simulations in which it is of interest to evaluate the boundary layer. It represents the dimensionless distance between the object wall and the first mesh cell. Its value affects the choice of the turbulence model to be used in the simulation, since different models perform better in different ranges of values of y^+ (Versteeg and Malalasekera, 2007).

Generally, the selection of the y^+ value is contingent upon the type of flow being simulated. For flows with high turbulence intensity, it is common to choose smaller values (on the order of 1), to better capture the regions close to the wall. For laminar flows or flows with low turbulence, higher values of y^+ (in the order of 30 to 200) can be used (Versteeg and Malalasekera, 2007).

As mentioned above, determining the value of y^+ is related to the discretization of the mesh used in the simulation. For

Table 1. Mesh convergence study.

Mesh	y^+ max	Number of nodes in the mesh in the highlighted directions				Cells
		Surface	Orthogonal		Wake direction	
			On BL	Outside BL		
1	1.091243	275	52	55	100	152226
2	1.075734	350	52	55	100	176001
3	1.065443	425	52	55	100	199776
4	1.047714	500	52	55	100	223551

structured meshes, it is possible to calculate it from the cell size and the velocity gradient in the direction normal to the wall (Ferziger and Peric, 2012). The adjustment could be made through the number of nodes in the direction orthogonal to the wall in the boundary layer region, having been set at 52 to find the corresponding maximum values of y^+.

To better denote the accuracy of the results generated by mesh refinement, the lift coefficient obtained for each case was compared. The percentage variation of the observed values in comparison with the C_l of 1.145 (reference value compared to the experimental case evaluated by McGhee *et al.* (1988), for which the value of 1.142 is presented), obtained for the most refined case (Mesh 4) made for a RANS-type simulation, with the Spalart-Allmaras model, is expressed in Figure 4.

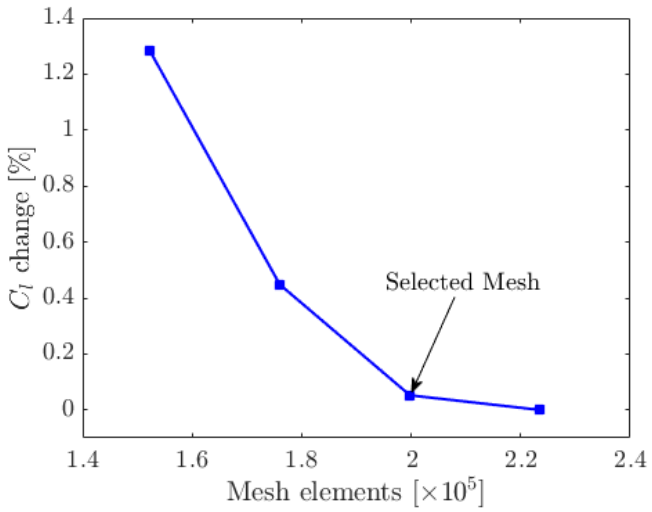

Figure 4. Percent change in C_l as a function of mesh resolution for the Eppler 387 airfoil with $\alpha = 8°$ and Re = 6×10^4.

The analysis of the percentage variation of the lift coefficient shows that, for all the proposed meshes, there is a relatively small variation of the response parameters. In particular, between Meshes 3 and 4 this variation becomes insignificant, denoting the independence of the results with the degree of refinement of the mesh.

Once the domain was defined, the numerical resolution of the flow governing equations was performed through numerical simulations performed in *software* OpenFoam. For the case study, the flow configurations were defined assuming Reynolds values of 6×10^4 and 4.5×10^4, considering the laminar and turbulent cases. The turbulent case was defined for a RANS (*Reynolds-Averaged Navier-Stokes*) simulation with a Spalart-Allmaras turbulence model, and the Direchlet and Newmann boundary conditions were appropriately selected for the airfoil boundaries and surface.

The post-processing of data obtained from the simulation in OpenFoam was carried out using *software* Paraview, a visualization and data analysis tool for computer simulations that allows the analysis of field contours that represent flow properties, such as velocity and pressure, in addition to allowing the visualization of streamlines.

4. RESULTS AND DISCUSSION

The RANS-type simulation, with consideration of the Spalart-Allmaras model, was integrated, in the first instance, due to the greater stability brought to the numerical simulation by the turbulence model. The consideration of this allowed the convergence of the analysis for the residual residuals (less than 1×10^{-5}), culminating in an adequate representation of the relevant magnitudes.

Figure 5 elucidates the pressure and horizontal velocity fields on the Eppler 387 airfoil for the configuration with an

angle of attack of $\alpha = 8°$ and $Re = 6 \times 10^4$. Streamlines are also illustrated to show the behavior of the flow as it travels across the airfoil surface.

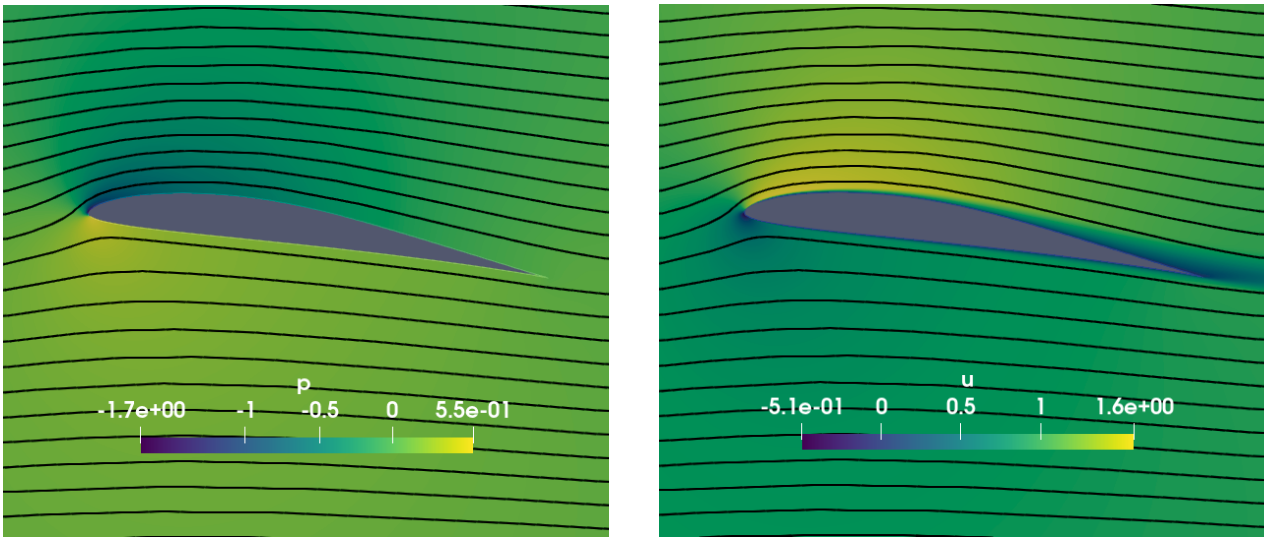

(a) (b)

Figure 5. Fields of (a) pressure and (b) horizontal velocity along the streamlines over the Eppler 387 airfoil, with $\alpha = 8°$ and $Re = 6 \times 10^4$, for RANS flow.

For comparison purposes, the configuration with an angle of attack of $\alpha = 8°$ and $Re = 4.5 \times 10^4$ was also evaluated, with the fields of interest illustrated in Figure 6.

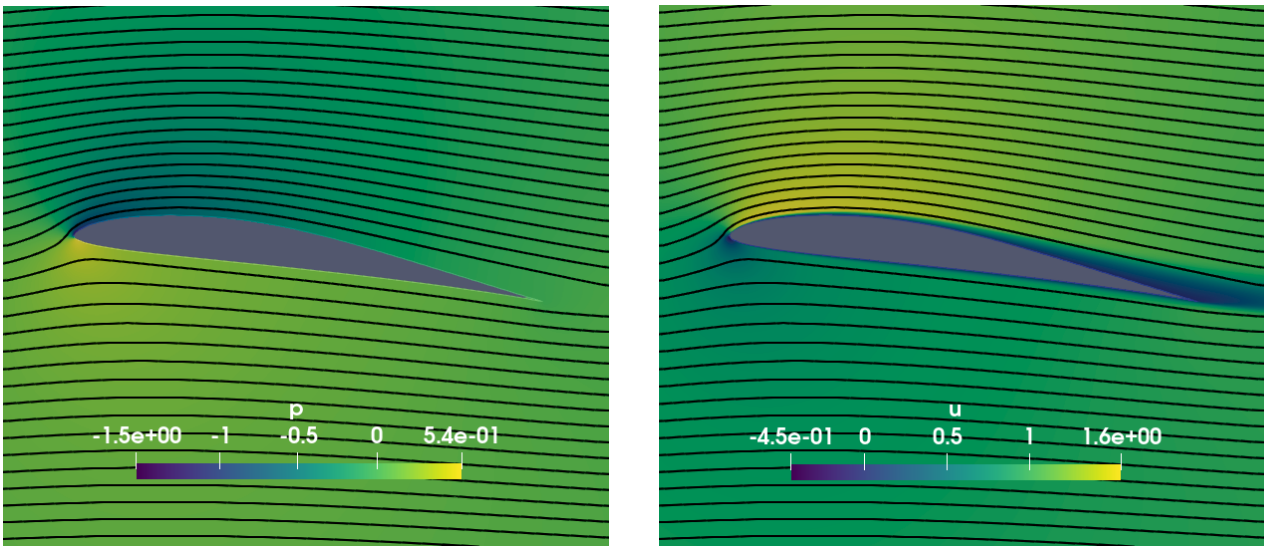

(a) (b)

Figure 6. Fields of (a) pressure and (b) horizontal velocity along the streamlines over the Eppler 387 airfoil, with $\alpha = 8°$ and $Re = 4.5 \times 10^4$, for RANS flow.

In order to validate the proposed numerical model, the distributions of pressure characteristics for such circumstances are represented in Figure 7, which highlights a comparative evaluation of the received curve with a similar case implemented in *software* XFLR5. For this comparison, an analysis via XFLR5 was performed forcing the boundary layer transition and separation on the leading edge, aiming at the maximum approximation with the case simulated by OpenFoam.

The consideration of the laminar flow, in turn, allows the representation of the flow adherent to the wall and, therefore, makes it possible to characterize the boundary layer and identify the phenomena that lead to the formation of the laminar separation bubble. For this case, however, an oscillation is observed for each variable of interest in the convergence history, characterized by the emission of vortices in the velocity and pressure fields, illustrated in Figure 8.

According to Mo and Rho (2020), the occurrence of the oscillation phenomenon is associated with unstable physical

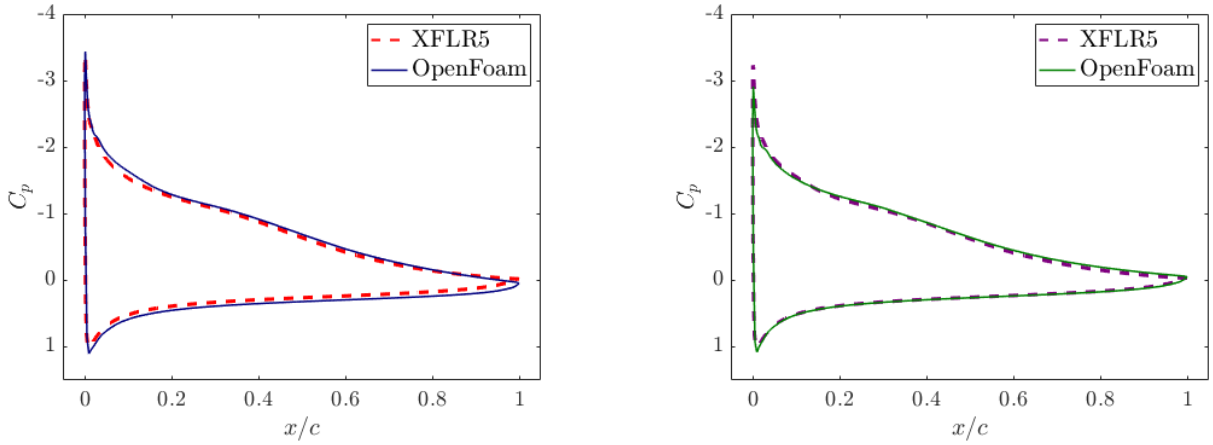

(a) (b)

Figure 7. Comparison of typical pressure distribution for separate (turbulent) flow: (a) $Re = 6\times10^4$ and (b) $Re = 4.5\times10^4$.

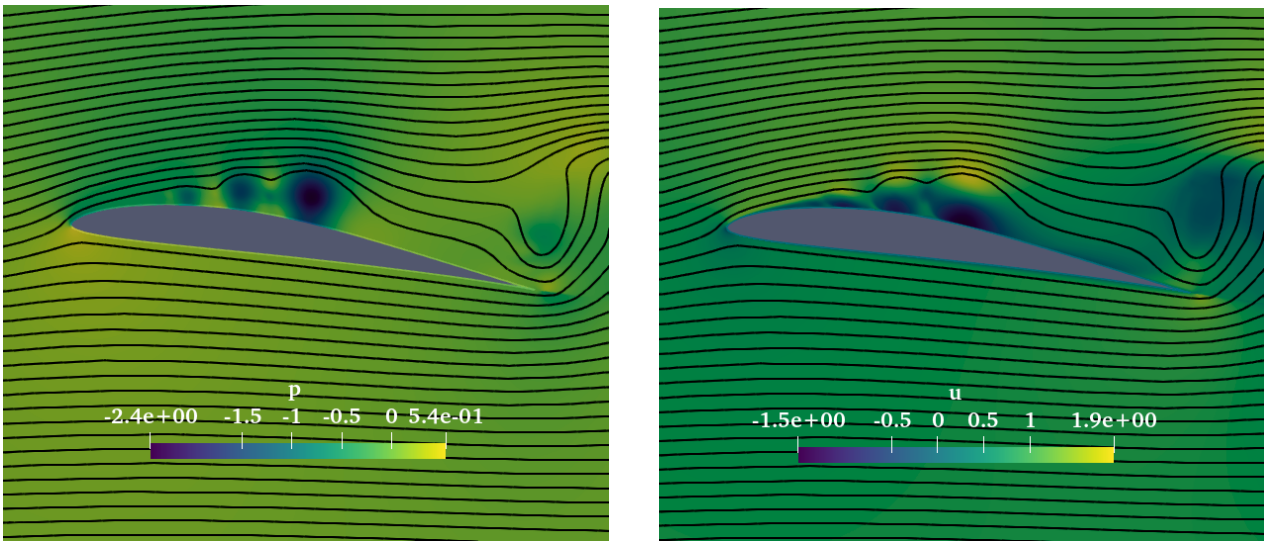

(a) (b)

Figure 8. Fields of (a) pressure and (b) horizontal velocity along the streamlines over the Eppler 387 airfoil, with $\alpha = 8°$ and $Re = 6 \times 10^4$, for laminar flow.

flow characteristics, being, in general, natural in flows with transition limited by surfaces in which there are separation bubbles, especially when the convergence criterion becomes very low. Mo and Rho (2020) assert that the average of the latest data is a reasonable method to accurately predict the aerodynamic coefficients, being a very valid alternative.

The laminar separation bubble can be evaluated from the skin friction coefficient obtained (Cebeci *et al.*, 1972). The separation point of a flow can be interpreted as the point at which the coefficient of friction on the contact surface is zero. Furthermore, the region denoting the LBS is demarcated by the negative part of the shear layer, so that the difference between its reattachment and separation points denotes the bubble length. Figure 9 shows this analysis for simulated cases.

For the evaluated cases, the formation of a short LSB is verified for Re = 6×10^4, with separation at 0.148c and reattachment at 0.464c (in terms of the airfoil chord, c). The characterization of this bubble as short is due to its influence on the distribution of laminar pressure compared to the corresponding distribution for an inviscid case, since a small plateau is identified arising from the presence of the region of recirculation of the bubble.

In turn, for Re = 4.5×10^4 a long LSB is obtained, with separation at 0.173c and reattachment at 0.682c. In this case, it is a long bubble due to its characteristic of moving the pressure distribution typical of the invisible curve more significantly away from the suction side, generating a larger plateau due to the more intense adverse pressure gradient. Figure 10 illustrates the pressure distributions for each case (the experimental case, evaluated by McGhee *et al.* (1988), is shown for comparison purposes).

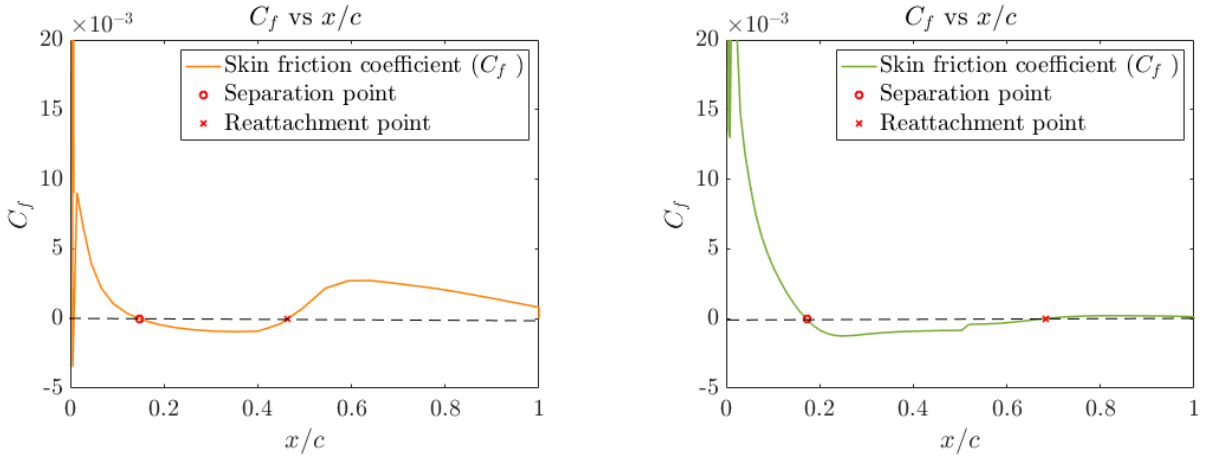

Figure 9. Identification of the laminar separation bubble from the skin friction coefficient: (a) $Re = 6 \times 10^4$ and (b) $Re = 4.5 \times 10^4$.

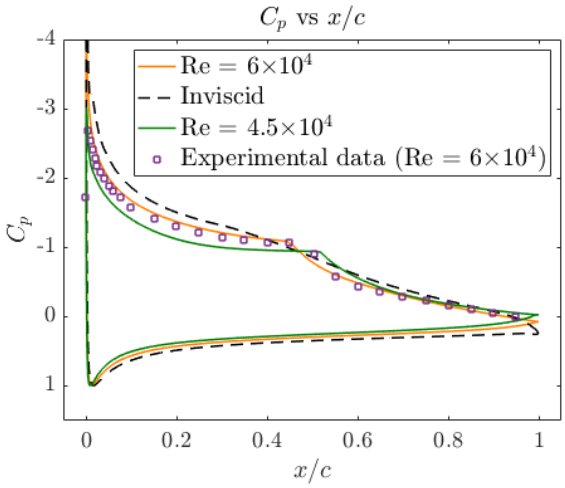

Figure 10. Typical pressure distribution for inviscid and laminar cases with Re = 6×10^4 and Re = 4.5×10^4.

5. CONCLUSIONS

In this work, we explore a practical methodology for analyzing the flow around an aerodynamic profile in order to observe the formation of laminar separation bubbles (LSB) and identify their aspects. The Eppler 387 airfoil was used to perform numerical simulations using the XFLR5 software and OpenFoam CFD code with the Spalart Allmaras model.

From the analyzes it was possible to identify characteristics such as the separation point and the reattachment point of the bubble. Furthermore, the pressure distributions along the surface were compared through different numerical simulations (including with experimental data), in steady state, showing its influence on the suction side.

The dependence of the location and size of the bubble on the Reynolds number was verified. For Re = 6×10^4 the formation of a short separation bubble was observed, while for Re = 4.5×10^4 a long bubble was identified. It is concluded that the reduction in the Reynolds number led to the bubble bursting, a phenomenon that directly affects the aerodynamic characteristics of the profile, as observed when comparing the pressure distributions for each case.

Finally, it should be noted that evaluating the behavior of this type of instability under the established conditions can be decisive understand its transition (bursting phenomena) and optimize forecasting and control methods. Therefore, the results denote great possibilities of contribution to the aeronautical industry, paving the way for the proposition of alternative techniques for stall control.

6. ACKNOWLEDGEMENTS

This study was financed in part by the Coordenação de Aperfeiçoamento de Pessoal de Nível Superior – Brasil (CAPES) – Finance Code 001

7. REFERENCES

Avanci, M.P., Rodríguez, D. and Alves, L.S.d.B., 2019. "A geometrical criterion for absolute instability in separated boundary layers". *Physics of Fluids*, Vol. 31, No. 1, pp. 014103–1–014103–11.

Balzer, W. and Fasel, H.F., 2016. "Numerical investigation of the role of free-stream turbulence in boundary-layer separation". *Journal of Fluid Mechanics*, Vol. 801, pp. 289 – 321.

Blazek, J., 2015. *Computational Fluid Dynamics: Principles and Applications*. Elsevier, Amsterdam, 3rd edition. ISBN 0080999956.

Burgmann, S. and Schroder, W., 2008. "Investigation of the vortex induced unsteadiness of a separation bubble via time-resolved and scanning PIV measurements". *Experiments in Fluids*, Vol. 45, No. 675, p. 675–691.

Cebeci, T., Mosinskis, G. and Smith, A.M., 1972. "Calculation of separation points in incompressible turbulent flows". *Journal of Aircraft*, Vol. 9, No. 9, pp. 618–624.

Diwan, S.S., Cheatan, S.J. and Ramesh, O.N., 2006. "Iutam symposium on laminar-turbulent transition: On the bursting criterion for laminar separation bubbles". In *Fluid Mechanics and Its Applications*. Dordrecht, Vol. 78, p. 401–407. ISBN 978-1-4020-3459-6.

Eppler, R., 2013. *Airfoil Design and Data*. Springer Science & Business Media, Dordrecht, Netherlands.

Ferziger, J.H. and Peric, M., 2012. *Computational Methods for Fluid Dynamics*. Springer, Berlin, 3rd edition. ISBN 978-3-642-21581-0.

Gaster, M., 1963. *On the Stability of Parallel Flows and the Behavior of Separation Bubbles*. Ph.D. thesis, Queen Mary College, Londres.

Geuzaine, C. and Remacle, J.F., 2009. "Gmsh: A 3-d finite element mesh generator with built-in pre- and post-processing facilities". *International Journal for Numerical Methods in Engineering*, Vol. 79, No. 11, pp. 1309–1331.

Hirsch, C., 2007. *Numerical Computation of Internal and External Flows*. Fundamentals of Computational Fluid Dynamics. Butterworth-Heinemann, Oxford, UK, 2nd edition. ISBN 9780750665940.

Katz, J. and Plotkin, A., 2001. *Low-Speed Aerodynamics*. 13. Cambridge University Press, New York, 2nd edition. ISBN 0-521-66219-2.

McGhee, R.J., Walker, B.S. and Millard, B.F., 1988. "Experimental results for the eppler 387 airfoil at low reynolds numbers in the langley low-turbulence pressure tunnel". Technical report, Langley Research Center, Hampton, Virginia.

Melvill Jones, B., 1934. "Stalling". *The Aeronautical Journal*, Vol. 38, No. 285, pp. 753 – 770.

Mitra, A. and Ramesh, O.N., 2019. "New Correlation for the Prediction of Bursting of a Laminar Separation Bubble". *AIAA Journal*, Vol. 57, No. 4, pp. 1400 – 1408.

Mo, J. and Rho, B., 2020. "Characteristics and effects of laminar separation bubbles on nrel s809 airfoil using the γ-re_θ transition model". *Applied Sciences*, Vol. 10, No. 6065, pp. 1–18.

Moukalled, F., Mangani, L. and Darwish, M., 2015. *The Finite Volume Method in Computational Fluid Dynamics: An Advanced Introduction with OpenFOAM® and Matlab*. Springer International Publishing, Switzerland, 1st edition. ISBN 3319168738.

Passaggia, P.Y., Leweke, T. and Ehrenstein, U., 2012. "Transverse instability and low-frequency flapping in incompressible separated boundary layer flows: an experimental study". *Journal of Fluid Mechanics*, Vol. 703, pp. 363–373.

Patankar, S.V., 1980. *Numerical Heat Transfer and Fluid Flow*. Series in computational methods in mechanics and thermal sciences. Hemisphere Pub. Corp., New York, NY, 1st edition. ISBN 0891165223.

Patankar, S.V. and Spalding, D.B., 1972. "A calculation procedure for heat, mass and momentum transfer in three-dimensional parabolic flows". *International Journal of Heat and Mass Transfer*, Vol. 15, No. 10, pp. 1787–1806.

Pier, B., 2002. "On the frequency selection of finite-amplitude vortex shedding in the cylinder wake". *Journal of Fluid Mechanics*, Vol. 458, p. 407–417.

Rodríguez, D., Gennaro, E. and Souza, L., 2021. "Self-excited primary and secondary instability of laminar separation bubbles". *Journal of Fluid Mechanics*, Vol. 906, p. A13.

Spalart, P. and Allmaras, S., 1992. *One-equation turbulence model for aerodynamic flows*. Recherche Aerospatiale, Palaiseau, 1st edition.

Versteeg, H.K. and Malalasekera, W., 2007. *An introduction to computational fluid dynamics: the finite volume method*. Pearson education, Harlow, England, 2nd edition. ISBN 9780131274983.

Zhao, Y. and Sandberg, R., 2020. "Bypass transition in boundary layers subject to strong pressure gradient and curvature effects". *Journal of Fluid Mechanics*, Vol. 888, p. A4.

Çengel, Y.A. and Cimbala, J.M., 2013. *Fluid Mechanics: Fundamentals and Applications*. Mechanical Engineering. McGraw-Hill Education, New York, 3rd edition. ISBN 978-0073380322.

8. RESPONSIBILITY NOTICE

The authors are solely responsible for the printed material included in this paper.